Optics Letters

Stimulated Brillouin scattering in layered media: nanoscale enhancement of silicon

M. J. A. Smith,[1,2,*] C. Wolff,[3] C. G. Poulton,[2] and C. Martijn de Sterke[1]

[1]Institute of Photonics and Optical Science (IPOS), School of Physics, The University of Sydney, NSW 2006, Australia
[2]School of Mathematical and Physical Sciences, University of Technology Sydney, NSW 2007, Australia
[3]Center for Nano Optics, University of Southern Denmark, Campusvej 55, DK-5230 Odense M, Denmark
*Corresponding author: michael.j.smith@sydney.edu.au

Received 29 November 2018; revised 20 January 2019; accepted 11 February 2019; posted 13 February 2019 (Doc. ID 353028); published 12 March 2019

We report a theoretical study of stimulated Brillouin scattering (SBS) in general anisotropic media, incorporating the effects of both acoustic strain and local rotation. We apply our general theoretical framework to compute the SBS gain for layered media with periodic length scales smaller than all optical and acoustic wavelengths, where such composites behave like homogeneous anisotropic media. We predict that a layered medium composing nanometer-thin layers of silicon and As_2S_3 glass has a bulk SBS gain of 1.28×10^{-9} W^{-1} m. This is more than 500 times larger than that of silicon and almost double the gain of As_2S_3. The enhancement is due to a combination of roto-optic, photoelastic, and artificial photoelastic contributions in the composite structure.

https://doi.org/10.1364/OL.44.001407

Interactions between photons and phonons represent an important avenue of research in photonics and optomechanics [1–3], not only for the transmission of light in optical fibers [4,5], but also for efficient, small-scale optical devices [6]. One of the most important effects for driving these interactions is stimulated Brillouin scattering (SBS) [5]. In bulk materials, SBS is frequently described as the resonant excitation of the first acoustic pressure mode of the medium by the optical pump field; the pressure wave acts as a traveling diffraction grating which scatters the pump and induces a Doppler-shifted returning (Stokes) wave. However, this description only holds in optically isotropic media where bulk SBS interactions are only possible with longitudinal acoustic waves and not with shear acoustic waves. In optically anisotropic materials, shear acoustic waves and mixed polarized acoustic waves are also SBS-active [7–9], due to reduced symmetry constraints. Here we consider SBS in this more general sense, defining the process as the inelastic resonant excitation of a bulk acoustic mode by the pump wave, leading to the formation of a backwards-propagating optical Stokes wave. A key issue with SBS in technologically relevant materials platforms, such as silicon, is intrinsically low SBS gain, which motivates considerable interest in novel designs for its enhancement (e.g., [1]). Composite materials have recently been explored theoretically as a means of controlling SBS [10–14]; however, layered structures are much more easily fabricated over other composite designs, and may be realized using existing semiconductor coating technology.

In this Letter, we report the results for SBS in a layered medium, as shown in Fig. 1 where in addition to photoelastic processes (including artificial photoelasticity [15]; see below), we have contributions to the SBS gain from induced optical anisotropy. By incorporating all relevant optoacoustic processes, we show that the gain coefficient of homogenized layered media takes values well above the SBS gain of the constituents in bulk. To demonstrate this point, for a Si–As_2S_3 layered medium, we find a gain coefficient of $g_P = 1.28 \times 10^{-9}$ W^{-1} m. This is two orders of magnitude larger than that of pure Si⟨100⟩ ($g_P = 2.4 \times 10^{-12}$ W^{-1} m [12]), 75% larger than that of pure As_2S_3 ($g_P = 0.714 \times 10^{-9}$ W^{-1} m [16]), and an order of magnitude larger than the results for a suspension of As_2S_3 spheres in Si ($g_P = 0.106 \times 10^{-9}$ W^{-1} m [13]). The enhancements are due to changes in the effective permittivity under changes in the filling fraction (*artificial photoelastic* contributions [10]), as well as changes to the permittivity under infinitesimal rotation (*roto-optic* contributions [7,17–20]), which are present, in addition to intrinsic photoelastic contributions from the layers [15].

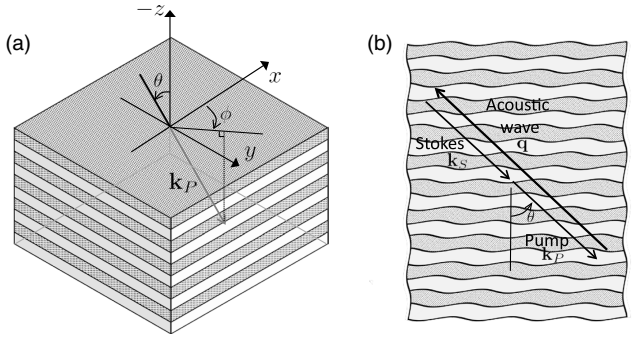

Fig. 1. (a) Illustration of composite bulk medium composing As_2S_3 glass (white) and silicon (gray) layers with (b) a cross-sectional view showing pump $\mathbf{k}_P$, Stokes $\mathbf{k}_S$, and acoustic $\mathbf{q}$ wave vectors involved in bulk backwards SBS interaction.

Although roto-opticity is not new [17], it is much less well known than conventional photoelasticity, as rotationally induced birefringence is not observed in materials of high symmetry. Artificial photoelastic effects are much more recent [10]. Within this Letter, care must be taken to avoid confusion regarding optoacoustic surface contributions at dielectric interfaces. We include all surface terms appearing within each unit cell in our effective medium treatment. Such terms are "microscopic" surface effects and are captured by the artificial electrostriction term. They should not be confused with "macroscopic" surface pressures that would arise between the composite and a possible cladding (e.g., in a waveguide structure). In our Letter (bulk composite material), there is no such cladding and, hence, no macroscopic boundary terms appear, although microscopic surface terms are fully captured in bulk expressions. All microscopic-scale interactions are implicitly captured in the effective medium treatment and are contained within the artificial electrostriction contributions (see Smith *et al.* [15]). The nontrivial relationship between radiation pressure and artificial electrostriction is demonstrated by the fact that artificial contributions vanish in the absence of either a permittivity or stiffness contrast [15], whereas radiation pressure effects vanish in the absence of only a permittivity contrast [21]. In materials possessing optical isotropy and acoustic anisotropy, such as germanium, a material frame rotation has been shown to improve the confinement of longitudinal acoustic modes for SBS [22].

We now generalize the coupled-mode approach in Wolff *et al.* [21] for evaluating the SBS gain of uniform anisotropic media. Assuming linear optical and acoustic properties, the SBS gain coefficient (in the absence of irreversible forces) is defined as [21]

$$g_{\mathrm{P}} = \frac{2\omega\Omega\gamma^2}{\mathcal{I}_{\mathrm{P}}\mathcal{I}_{\mathrm{S}}\mathcal{I}_{\mathrm{A}}\alpha}, \tag{1}$$

where γ (units [Pa]) denotes the total electrostrictive coefficient, $\mathcal{I}_{\mathrm{P}}$ is the pump intensity (units [W/m^2]), $\mathcal{I}_{\mathrm{S}}$ is the Stokes intensity (units [W/m^2]), and $\mathcal{I}_{\mathrm{A}}$ is the acoustic intensity (units [W/m^2]), where all intensities are associated with the modes of the optical and acoustic waves in the material. Here α is the acoustic attenuation constant (units [1/m]). These are given by

$$\gamma = -\varepsilon_0\varepsilon_{im}\varepsilon_{jn}P_{mnkl}(\partial_l u_k)^*E_i^{\mathrm{P}}(E_j^{\mathrm{S}})^*, \tag{2a}$$

$$\mathcal{I}_{\mathrm{P}} = 2(\hat{v}_{\mathrm{g}}^{\mathrm{P}})_i\epsilon_{ijk}(E_j^{\mathrm{P}})^*H_k^{\mathrm{P}}, \tag{2b}$$

$$\mathcal{I}_{\mathrm{S}} = 2(\hat{v}_{\mathrm{g}}^{\mathrm{P}})_i\epsilon_{ijk}(E_j^{\mathrm{S}})^*H_k^{\mathrm{S}}, \tag{2c}$$

$$\mathcal{I}_{\mathrm{A}} = -2\mathrm{i}\Omega(u_i)^*(\hat{v}_{\mathrm{g}}^{\mathrm{P}})_jC_{ijkl}s_{kl}, \tag{2d}$$

$$\alpha = \Omega^2\mathcal{I}_{\mathrm{A}}^{-1}s_{ij}\eta_{ijkl}(s_{kl})^*, \tag{2e}$$

where ε_{ij} is the relative permittivity tensor, u_k is the acoustic displacement from equilibrium, and $E^{\mathrm{P,S}}$ and $H^{\mathrm{P,S}}$ are the electric and magnetic field vectors for the pump and Stokes fields, respectively. Additionally, $\hat{v}_{\mathrm{g}}^{\mathrm{P}}$ is the normalized group velocity for the pump field, ϵ_{ijk} is the Levi–Civita tensor, C_{ijkl} is the stiffness tensor, and η_{ijkl} is the phonon viscosity tensor. Finally, ω and Ω are the angular frequencies of the pump field and the acoustic wave, respectively, and $s_{kl} = (\partial_k u_l + \partial_l u_k)/2$ is the linear strain tensor. Here we define P_{ijkl} via [23]

$$\Delta\varepsilon_{ij} = -\varepsilon_{im}\varepsilon_{jn}P_{(mn)kl}\partial_l u_k, \tag{3a}$$

where the full photoelastic tensor decomposes as

$$P_{(ij)kl} = p_{(ij)(kl)} + p_{(ij)[kl]}, \tag{3b}$$

for non-piezoelectric dielectric materials, with $p_{(ij)(kl)}$ and $p_{(ij)[kl]}$ denoting the symmetric and antisymmetric (roto-optic) photoelastic tensors, respectively. Following Ref. [23], we represent index pair interchange symmetry with parentheses and interchange antisymmetry with square brackets. Note that Eq. (3b) represents a key departure from conventional treatments of SBS, as $p_{(ij)[kl]} \equiv 0$ in optically isotropic materials [24].

To evaluate Eq. (1), it is necessary to determine a large number of modal fields belonging to several different families. For determining the optical fields and quantities in Eq. (2), such as wave polarizations and the refractive index, we consider Maxwell's equations with the plane wave ansatz $E_j = \tilde{E}_j\exp(\mathrm{i}k_ix_i - \mathrm{i}\omega t)$ where $\tilde{E}_j$ denotes the polarization of the wave, and k_j is the wave vector. This ansatz admits the system [25]

$$\left(\hat{k}_i\hat{k}_j - \left(1 - \frac{\varepsilon_j}{n^2}\right)\delta_{ij}\right)\tilde{E}_j = A_{ij}^{\mathrm{M}}\tilde{E}_j = 0, \tag{4}$$

where $k_i = k\hat{k}_i$, $k = n\omega/c_0$ is the wave number, n is the refractive index, and c_0 denotes the speed of light in vacuum. Subsequently, for a given wave vector k_j, the supported refractive indices are obtained by solving $\det(A^{\mathrm{M}}) = 0$ and the associated eigen-polarizations $\tilde{E}_j$ are given by the eigenvectors of A^{M}. The corresponding group velocity of the wave ($[v_g]_i = \partial_{k_i}\omega$) is obtained by implicit differentiation of Eq. (4).

In order to determine the properties of the available Stokes waves for a given pump wave vector k_j^{P}, namely the wave vectors k_j^{S} and wave polarizations $\tilde{E}_j^{\mathrm{S}}$, we impose that the direction of the group velocity vector for the Stokes wave is opposite in sign to that of the pump wave ($[\hat{v}_g^{\mathrm{S}}]_j = -[\hat{v}_g^{\mathrm{P}}]_j$), which is consistent with backwards SBS coupling. From this group velocity condition, the properties of the Stokes wave are obtained following the procedure above for the pump wave.

To determine acoustic fields and quantities, we consider the acoustic wave equation [8] assuming the plane wave ansatz $u_j = \tilde{u}_j\exp(\mathrm{i}q_ix_i - \mathrm{i}\Omega t)$, where $\tilde{u}_j$ is the polarization, and the acoustic wave vector q_j is defined by $q_j = k_j^{\mathrm{P}} - k_j^{\mathrm{S}} = q\hat{q}_j$ [4,5]. Subsequently, we obtain the eigenvalue problem

$$A_{ij}^{\mathrm{A}}v_j = \frac{\rho\Omega^2}{q^2}v_i, \tag{5}$$

which returns $\rho\Omega^2/q^2$ as eigenvalues and $\tilde{u}_j$ as eigenvectors, where ρ denotes the mass density, and $v_j = \partial_t u_j$ the phase velocity of the wave. The Christoffel tensor A_{ij}^{A} is widely tabulated for a broad selection of Bravais lattice classes [8,26,27].

We now present a numerical study of the SBS performance of Si-As_2S_3 layered media with a unit cell length of 50 nm at a wavelength $\lambda_0 = 1550$ nm. Even though the layered media consists of acoustically isotropic (As_2S_3) and cubic (Si) materials, the composite medium is optically uniaxial. In Eqs. (1)–(3b) above, we use closed-form expressions for ε_{ij}, C_{ijkl}, η_{ijkl}, ρ, and $P_{(ij)kl}$ [15] for laminate materials with tetragonal ($4/mmm$) symmetry (i.e., when the constituent layers are isotropic or cubic). These descriptions are valid provided the wavelengths of all optical and acoustic waves are much longer than the periodic length scale of the laminate; in this regime, the composite material behaves as an effective

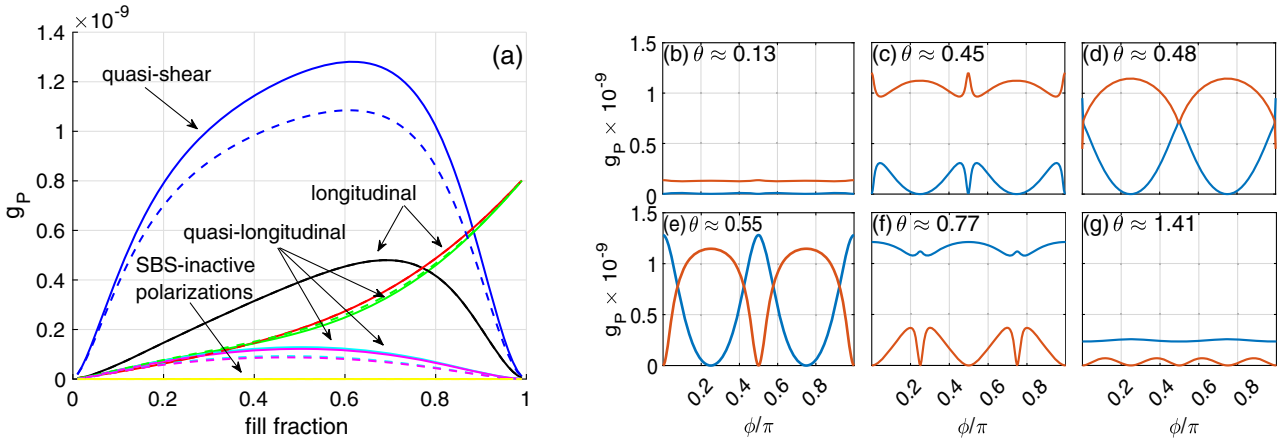

Fig. 2. SBS gain coefficient for As_2S_3-Si layered medium as (a) a function of filling fraction f for the fixed pump wave vector $k^P \approx (0.52, 0, 0.85)$. The dashed curves are gain values when roto-optic contributions are neglected (i.e., $p_{ij[kl]} = 0$). Each curve represents different combinations (branches) of pump, Stokes, and acoustic waves (i.e., blue = quasi-shear, red = longitudinal acoustic wave polarizations); (b)–(g) functions of $k^P = (\sin\theta\cos\phi, \sin\theta\sin\phi, \cos\theta)$ at $f \approx 0.61$. Two competing mixed acoustic mode branches are shown (remaining branches omitted for clarity). In all figures, we consider a period of 50 nm.

uniform material. The material constants for the constituent layers are given in Smith *et al.* [12].

The laminates we consider generally support two pump waves for wave vectors oriented away from directions of high symmetry (one for the extraordinary and another for the ordinary surface). Thus, for a specified $\hat{k}^P$ in a bulk uniaxial crystal, up to four pair combinations of pump and Stokes waves may contribute to an SBS process. For each combination of pump and Stokes wave field, there are up to three acoustic wave polarizations supported at long wavelengths, giving a total of 12 possible combinations of pump, Stokes, and acoustic waves to participate in an SBS process in a tetragonal $(4/mmm)$ material for a given $\hat{k}^P$. In a composite material, the symmetric photoelastic tensor in Eq. (3b) may be decomposed further as

$$p_{(ij)(kl)} = p^{pe}_{(ij)(kl)} + p^{art}_{(ij)(kl)}, \tag{6}$$

representing some weighted average of constituent photoelastic terms and artificial photoelasticity coefficients, respectively [15].

Figure 2(a) shows the gain coefficient versus filling fraction for all 12 possible combinations of pump, Stokes, and acoustic wave polarizations (henceforth, we refer to each of these 12 combinations as *branches*) corresponding to $k^P \approx (0.52, 0, 0.85)$. This wave vector corresponds to the maximum possible gain value of $\max(g_P) = 1.28 \times 10^{-9}$ W^{-1} m for this material pair, which occurs at $f \approx 0.61$ (note that two other k^P orientations return the same $\max(g_P)$; see below). The dashed lines superimposed on this figure are the 12 branches for this structure when roto-optic contributions are neglected, returning a maximum gain value of $g_P = 1.08 \times 10^{-9}$ W^{-1} m at $f \approx 0.61$ and, ultimately, revealing a roto-optic enhancement of 19% to $\max(g_P)$. These dashed curves also allow us to identify the shear contribution to each mode, revealing that the medium-gain branches [depicted by the black, red, and green curves in Fig. 2(a)] are almost purely longitudinal acoustic modes, for example. At filling fractions of approximately 88% and higher, the greatest gain value occurs for a longitudinally polarized acoustic mode (red curve), which is the only acoustic polarization that is SBS-active in isotropic materials. Recall that pure Si $\langle 100 \rangle$, i.e., $f = 0\%$, has weak SBS with $g_P = 2.4 \times 10^{-12}$ [12]. At $f = 100\%$, we obtain $g_P = 0.802 \times 10^{-9}$ W^{-1} m for pure As_2S_3, which is marginally higher than the experimental results ($g_P = 0.714 \times 10^{-9}$ W^{-1} m in As_2S_3) [16]. Note also that half of the available mode branches are not SBS-active for any filling fraction. If we decompose the total electrostrictive coefficient in Eq. (1) as $\gamma = \gamma^{pe} + \gamma^{art} + \gamma^{ro}$, corresponding, respectively, to the intrinsic, artificial, and roto-optic photoelastic contributions, we find that these quantities amount to 74%, 18%, and 8% of the overlap for the maximum gain in Fig. 2(a), respectively. The modest contributions γ^{art} and γ^{ro} are responsible for significant increases in the gain following Eq. (1), and highlight the importance of accurately capturing all optomechanical processes for SBS calculations in composites. To summarize, we find a maximum gain of $g_P = 1.28 \times 10^{-9}$ W^{-1} m at $k^P \approx (0.52, 0, 0.85)$ and $f \approx 0.61$, where $\Omega/(2\pi) = 8.4$ GHz, $\alpha = 16665$ m^{-1}, $v_g^A = 2353$ m/s, and $k^S = -k^P$. (The material tensors are summarized in Table 1.)

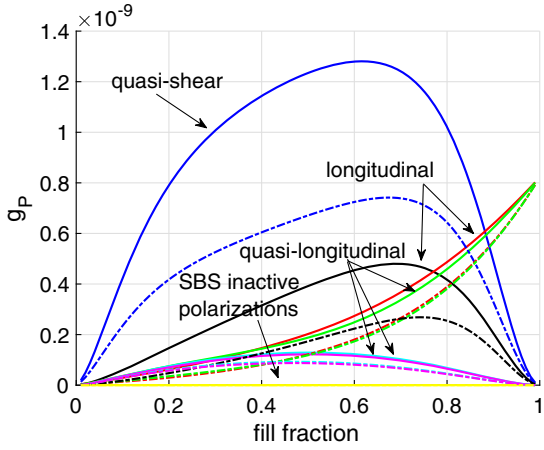

Fig. 3. SBS gain coefficient as a function of f for the As_2S_3-Si layered medium shown in Fig. 1(a), where results for neglected roto-optic and artificial photoelastic contributions (i.e., both $p_{ij[kl]} = 0$ and $p^{art}_{ij(kl)} = 0$) are overlaid (dotted–dashed curves).

Table 1. Bulk Values for Relative Permittivity ε_j, Stiffness C_{ij} (Units [GPa]), Phonon Viscosity η_{ij} (Units [mPa·s]), Density ρ (Units [kg · m^{-3}]), Symmetric Photoelastic $p_{i(j)}$, and Roto-Optic $p_{i[j]}$ Tensors of a Layered Medium ($f = 0.61$)[a]

Physical quantity	ε_1	ε_3	C_{11}	C_{33}	C_{13}	C_{12}	C_{44}	C_{66}	η_{11}	η_{33}	η_{13}	η_{12}	η_{44}	η_{66}	ρ
Effective parameter	8.11	7.08	68.2	28.4	9.9	21.1	9.9	34.6	2.63	2.46	2.05	2.13	0.25	0.35	2864

Physical quantity	$p_{1(1)}$	$p_{3(3)}$	$p_{1(3)}$	$p_{1(2)}$	$p_{3(1)}$	$p_{4(4)}$	$p_{6(6)}$	$p^{\text{art}}_{1(1)}$	$p^{\text{art}}_{3(3)}$	$p^{\text{art}}_{1(3)}$	$p^{\text{art}}_{1(2)}$	$p^{\text{art}}_{3(1)}$	$p_{4[4]}$
Effective parameter	0.015	0.258	0.143	0.107	0.209	−0.0004	−0.0422	0.012	0.03	0.031	0.012	0.012	0.009

[a]Subscripts are in Voigt form and $p_{i(j)} = p^{\text{pe}}_{i(j)} + p^{\text{art}}_{i(j)}$.

In Figs. 1(b)–1(g), we consider the gain coefficient at the fixed filling fraction $f \approx 0.61$ versus the pump wave vector, i.e., for $k^{\text{P}} = (\sin\theta\cos\phi, \sin\theta\sin\phi, \cos\theta)$, where ϕ is measured relative to the $\langle 100\rangle$ axis of Si, and the layers are stacked along $\langle 001\rangle$. Specifically, we present the gain along ϕ (equatorial plane): we sweep meridional angles θ. For clarity, we only show the two largest and competing branches. These figures show the importance of correctly orienting the pump wave vector: particular orientation angles correspond to gain suppression (i.e., at $\theta \approx 0.45$ and $\phi = \pi/2$), and the maximum gain occurs at multiple pump wave directions, corresponding to $\phi = 0, \pi/2, \pi$ with $\theta \approx 0.55$. For $\theta \approx 0.55$, the maximum gain branch (blue curve) shows that the incident wave vector must be appropriately oriented to achieve the maximum results; however, the presence of the second acoustic branch (red curve) ensures that the gain coefficient does not take values below $g_{\text{P}} \approx 0.78 \times 10^{-9}$ W^{-1} m. All figures demonstrate the intense competition between acoustic mode branches for the maximum gain position, in addition to revealing intrinsic symmetries for the gain parameter in layered media as a function of the k^{P} direction.

Figure 3 shows the gain coefficient for the layered medium for $f = 0.61$ and along $k^{\text{P}} \approx (0.52, 0, 0.85)$, when both roto-optic and artificial photoelastic contributions are neglected. We have superimposed the total gain coefficient curves from Fig. 2(a) for reference. Note that the estimated gain for layered media in the absence of these two contributions is significantly reduced (the maximum gain occurs at $f \approx 0.67$ with $g_{\text{P}} = 0.74 \times 10^{-9}$ W^{-1} m). At $f \approx 0.61$, we find $g_{\text{P}} = 0.73 \times 10^{-9}$ W^{-1} m, indicating that artificial and roto-optic effects increase the maximum SBS gain coefficient by approximately 75%.

In summary, we present a theoretical framework for investigating SBS in anisotropic materials. Using this framework, we show that a nanoscale layered material, consisting of Si and As_2S_3, has an SBS coefficient that outperforms leading uniform materials and larger than that of either constituent material. This performance of this structure is achieved by incorporating contributions from the symmetric photoelastic tensor (containing artificial photoelastic contributions only present in composite media), as well as contributions from the antisymmetric photoelastic tensor (roto-optic tensor), which arises only in optically anisotropic media. We also show that artificial photoelastic and roto-optic contributions are non-negligible in optically anisotropic materials, contributing significantly to the total gain coefficient. We find that the gain coefficient of the layered medium is larger than that of a structure with arrays of embedded spheres [13], because the artificial contribution is stronger and because of the emergence of roto-optic contributions. We note that the design of a nanoscale physical devices needs to include effects from external boundaries including waveguide boundaries; these effects depend on the effective properties and SBS response of the layered bulk medium as presented here. Therefore, the framework presented here provides an extensive scope for the ongoing development of new materials for future photonics and optomechanics research.

Funding. Australian Research Council (ARC) (CE110001018, DP160101691); H2020 Marie Skłodowska-Curie Actions (MSCA) (713694).

REFERENCES

1. R. van Laer, B. Kuyken, D. van Thourhout, and R. Baets, Nat. Photonics **9**, 199 (2015).
2. O. Florez, P. F. Jarschel, Y. A. Espinel, C. Cordeiro, T. M. Alegre, G. S. Wiederhecker, and P. Dainese, Nat. Commun. **7**, 11759 (2016).
3. N. T. Otterstrom, R. O. Behunin, E. A. Kittlaus, Z. Wang, and P. T. Rakich, Science **360**, 1113 (2018).
4. R. W. Boyd, *Nonlinear Optics* (Elsevier, 2003).
5. P. E. Powers, *Fundamentals of Nonlinear Optics* (CRC Press, 2011).
6. P. T. Rakich, C. Reinke, R. Camacho, P. Davids, and Z. Wang, Phys. Rev. X **2**, 011008 (2012).
7. D. F. Nelson and P. D. Lazay, Phys. Rev. Lett. **25**, 1187 (1970).
8. B. A. Auld, *Acoustic Fields and Waves in Solids* (Wiley, 1973).
9. D. F. Nelson and P. D. Lazay, Phys. Rev. B **16**, 4659 (1977).
10. M. J. A. Smith, B. T. Kuhlmey, C. M. de Sterke, C. Wolff, M. Lapine, and C. G. Poulton, Phys. Rev. B **91**, 214102 (2015).
11. W. Sun, S. Wang, J. Ng, L. Zhou, and C. T. Chan, Phys. Rev. B **91**, 235439 (2015).
12. M. J. A. Smith, B. T. Kuhlmey, C. M. de Sterke, C. Wolff, M. Lapine, and C. G. Poulton, Opt. Lett. **41**, 2338 (2016).
13. M. J. A. Smith, B. T. Kuhlmey, C. M. de Sterke, C. Wolff, M. Lapine, and C. G. Poulton, J. Opt. Soc. Am. B **33**, 2162 (2016).
14. X.-X. Su, X.-S. Li, Y.-S. Wang, and H. P. Lee, J. Opt. Soc. Am. B **34**, 2599 (2017).
15. M. J. A. Smith, C. M. de Sterke, C. Wolff, M. Lapine, and C. G. Poulton, Phys. Rev. B **96**, 064114 (2017).
16. R. Pant, C. G. Poulton, D.-Y. Choi, H. Mcfarlane, S. Hile, E. Li, L. Thevenaz, B. Luther-Davies, S. J. Madden, and B. J. Eggleton, Opt. Exp. **19**, 8285 (2011).
17. R. A. Toupin, J. Ration. Mech. Anal. **5**, 849 (1956).
18. D. F. Nelson and P. D. Lazay, Phys. Rev. Lett. **25**, 1638 (1970).
19. D. F. Nelson, *Electric, Optic, and Acoustic Interactions in Dielectrics* (Wiley, 1979).
20. R. Vacher and E. Courtens, in *International Tables for Crystallography*, A. Authier, ed. (International Union of Crystallography, 2006), Vol. **D**, Chap. 2.4, pp. 329.
21. C. Wolff, M. J. Steel, B. J. Eggleton, and C. G. Poulton, Phys. Rev. A **92**, 013836 (2015).
22. C. Wolff, R. Soref, C. G. Poulton, and B. J. Eggleton, Opt. Exp. **22**, 30735 (2014).
23. D. F. Nelson and M. Lax, Phys. Rev. Lett. **24**, 379 (1970).
24. D. F. Nelson, P. D. Lazay, and M. Lax, Phys. Rev. B **6**, 3109 (1972).
25. M. Born and E. Wolf, *Principles of Optics: Electromagnetic Theory of Propagation, Interference and Diffraction of Light* (Pergamon, 1964).
26. J. F. Nye, *Physical Properties of Crystals: Their Representation by Tensors and Matrices* (Oxford University, 1985).
27. R. E. Newnham, *Properties of Materials: Anisotropy, Symmetry, Structure* (Oxford University, 2004).